CRYSTAL GROWTH & DESIGN

Article

pubs.acs.org/crystal

Biomineralization in Mediterranean Corals: The Role of the Intraskeletal Organic Matrix

Michela Reggi,[†] Simona Fermani,[†] Valerio Landi,[†] Francesca Sparla,[‡] Erik Caroselli,[§] Francesca Gizzi,[§] Zvy Dubinsky,[∥] Oren Levy,[∥] Jean-Pierre Cuif,[⊥] Yannicke Dauphin,[⊥] Stefano Goffredo,*[,§] and Giuseppe Falini*[,†,#]

[†]Dipartimento di Chimica "Giacomo Ciamician", via Selmi 2, [‡]Dipartimento di Farmacia e Biotecnologie, Via S. Donato 15, [§]Dipartimento di Scienze Biologiche, Geologiche e Ambientali, Sezione di Biologia, via Selmi 3, Alma Mater Studiorum - Università di Bologna, 40100 Bologna, Italy

[∥]The Mina and Everard Goodman Faculty of Life Sciences, Bar-Ilan University, Ramat-Gan 52900, Israel

[⊥]Université Paris-Sud, Orsay, Bat. 504, UMR IDES, F-91405 Orsay, France

[#]Centro Interdipartimentale di Ricerca per le Scienze Ambientali, Sede di Ravenna - Università di Bologna, via S. Alberto 163, 48100 Ravenna, Italy

Supporting Information

ABSTRACT: The precipitation of calcium carbonate was carried out in the presence of the intraskeletal organic matrix (OM) extracted from Mediterranean corals. They were diverse in growth form and trophic strategy, *Balanophyllia europaea* and *Leptopsammia pruvoti*—solitary corals, only the first zooxanthellate coral—and *Cladocora caespitosa* and *Astroides calycularis*—colonial corals, only the first zooxanthellate coral. The results showed that, although the OM marked differences among species, the diverse influence over the calcium carbonate precipitation was evident only for *B. europaea*. This OM was the most prone to favor the precipitation of aragonite in the absence of magnesium ions, according to overgrowth and solution precipitation experiments. In artificial seawater, where magnesium ions were present, this OM, as well the one from *A. calycularis*, precipitated mainly a form of amorphous calcium carbonate different from that obtained with SOM from *L. pruvoti* or *C. caespitosa*. The amorphous calcium carbonate from *B. europaea* was the most stable upon heating up to 100 °C and was the one that mainly converted into aragonite instead of magnesium calcite after heating at 300 °C. All this indicated a higher control of *B. europaea* OM over the calcium carbonate polymorphism than the other species. The influence of SOMs over precipitate morphology turned out to be also species related. In conclusion, this comparative study has shown that the influence of OM on *in vitro* precipitation of calcium carbonate was not related to the coral ecology, solitary vs colonial and zooxanthellate vs nonzooxanthellate, and suggested that the coral control over biomineralization process was species specific and encoded in coral genes.

INTRODUCTION

Scleractinian corals represent the biggest source of biogenic calcium carbonate[1,2] and are among the fastest marine mineralizing organisms.[3] In corals the calcification process occurs in a biological confined environment, under the control of biological macromolecules.[4] This is confirmed by the observation that, although coral skeleton morphology can be affected by habitat conditions,[5−7] the change always remains within the species-specific "vocabulary" controlled by the DNA of the organism.[8−10]

The skeleton of corals is a composite structure with both inorganic (aragonite) and organic components.[11,12] The merging of data from several investigations[13,14] has revealed that the actual growth unit of the skeleton is a few micrometers-thick mineralizing growth layer synchronically increasing the "sclerodermites", forming a given skeletal unit (e.g., a septum). The mineralizing growth layer simultaneously increases the two distinct mineralizing areas that have been extensively described from a structural point of view. At the growth edge of any structural components (e.g., septal spines) a granular and porous nanocrystalline phase (randomly oriented) forms the initial skeletal framework (also the earliest appearing mineralized elements after larval metamorphosis, according to Vandermeulen and Watabe[15]). These early mineralizing zones (EMZ), usually called "center of calcification", are laterally reinforced by deposition of a second structural layer made of dense, large, acicular crystals: the fibers.[16]

Organic components, referred to as organic matrix (OM), are involved in biomineral synthesis and become entrapped in the skeleton.[17−20] The composition of coral OM compounds

Received: March 13, 2014
Revised: June 9, 2014
Published: July 7, 2014

 © 2014 American Chemical Society dx.doi.org/10.1021/cg5003572 | Cryst. Growth Des. 2014, 14, 4310−4320

can be determined only after skeleton decalcification processes. On the basis of the studies performed by Young[12] and Constantz and Weiner[21] proteins and glycosaminoglycans but also sulfated polysaccharides[14,22] and lipids[23] are consistently found in the skeletons of many species covering the whole taxonomic scleractinian diversity (ref 9 and references therein). These molecules have a different role in the biomineral synthesis according to diverse biomineralization models. In physicochemical models, involving a liquid layer with chemical properties called calcifying fluid,[24] the OM acts as a support for calcium carbonate-oriented crystallization.[2] In these models crystal growth occurs through a primarily inorganic process, which involves a coral-controlled transcellular ion transport to the calcifying fluid (ref 9 and references therein). A recent model of ionic transport shows a direct and rapid seawater transport to the calcification site.[25] In contrast to physicochemical models, Clode and Marshall[26] have suggested a molecular model in which calcification occurs within a gel secreted at the interface between the calicoblastic cells and the skeleton. According to this model the glycoproteins form an architectural framework bearing the sites for development of the mineral phase.[27] In this model, OM interacts with the growing crystal changing its shape.[28−30] More recently, attention was drawn on the potential role of OM as carriers of the mineral precursors, which are possibly in an amorphous status. In this view, the OM became trapped along the boundary grains of the final crystal during the transition from the amorphous to the crystalline phase.[10,30]

Many aspects of the OM role in the dynamics of skeleton formation of corals are enigmatic.[4] It has been recently shown, by *in vitro* studies, that the OM from different corals species influences polymorphism and morphology of calcium carbonate. Goffredo et al.[31] showed that the intraskeletal OM from Mediterranean zooxanthellate solitary coral, *Balanophyllia europaea*, can favor the precipitation of aragonite and that a transient phase of amorphous calcium carbonate (ACC) stabilized by lipids is involved. The influence of coral intraskeletal OM molecules in the precipitation of calcium carbonate was proved also for the tropical species *Acropora digitifera*, *Lophelia pertusa*, and *Montipora caliculata*.[10] Moreover, an important recent study has shown that four highly acidic proteins, derived from the expression of genes obtained from the common coral *Stylophora pistillata* can spontaneously catalyze the precipitation of calcium carbonate *in vitro* from seawater.[32]

This study deepened the investigations using the OM from skeletons of *Leptopsammia pruvoti* (solitary, nonzooxanthellate), *Balanophyllia europaea* (solitary, zooxanthellate), *Astroides calycularis* (colonial, nonzooxanthellate), and *Cladocora caespitosa* (colonial, zooxanthellate). These Mediterranean coral species were chosen because they represent the combination among different growth forms and trophic strategies. Solitary corals are single autonomous individuals (polyps), while colonial corals are modular organisms constituted by cloned polyps living in close connection (physical and physiological) one to each other. Symbiosis determines the synthesis of molecules essential to the biomineralization process,[33] such as precursors for the OM.[9,34−36] The first link between photosynthesis and calcification was found by Kawaguti and Sakumoto;[37] they pointed out that calcification rate is higher in the light than in the dark.[9] It was also shown that in the presence of light the calcification rate is higher in zooxanthellate corals than in nonzooxanthellate corals.[38] However, from a general point of view, it is clear that coral calcification is not dependent on the presence of symbionts[39,40] and non-zooxanthellate corals have an efficient calcification as well. Moreover, tissues that calcify at the highest rates, or which initiate calcification, do not possess zooxanthellae.[9,41,42] It was also shown that photosynthesis increases calcification rate because it fixes CO_2 and increases the skeleton surface pH.[43−45]

The main goals of this study are (a) to evaluate whether the intraskeletal OM from different coral species shows a different capability to govern the formation and stability of calcium carbonate precipitates; (b) to infer possible relationships between the organism ecology (growth form and trophic strategy) and its OM capabilities.

MATERIALS AND METHODS

Coral Skeletons. The samples of *L. pruvoti*, *B. europaea*, *C. caespitosa* from Calafuria and *A. calycularis* from Palinuro (Italian coast, North-Western Mediterranean Sea) were randomly collected by scuba diving at 16, 6, and 9 m depth, respectively, between 1 July 2010 and 25 February 2012. Coral skeletons were cleaned, ground, and analyzed by X-ray powder diffraction using a powder diffractometer (PanAnalytical X'Pert Pro equipped with X'Celerator detector) with Cu Kα radiation. Thermogravimetric analysis (TGA) was performed to estimate the OM content in the coral skeleton using an SDT Q600 instrument (TA Instruments). These analyses were carried out as previously reported.[10]

Extraction of the Organic Matrix. The soluble (SOM) and the insoluble (IOM) OM fractions were extracted through decalcification using a 0.1 M CH_3COOH solution as previously reported.[10] The whole OM (*w*OM) was obtained using the same procedure without the separation step between SOM and IOM.

Characterization of the OM. The polyacrylamide gel electrophoresis (SDS-PAGE) of SOM was performed on 12.5% polyacrylamide gel, according to a reported procedure[10] that implies the use of strong fixative agents. The PAS (Periodic Acid Schiff) stain was performed to detect glycoprotein.

Amino acid analysis (AAA) was conducted by a chromatographic technique using an amino acid analyzer, according to a reported procedure.[10] The average protein pI of all the OM fractions was calculated from the amino acid analyses of all the species, following the method described in Sillero and Ribeiro.[46]

Aliquots of OM fractions and *w*OM were analyzed by Fourier transform infrared spectroscopy (FTIR) using a FTIR Nicolet 380 Thermo Electron Corporation working in the range of wavenumbers 4000−400 cm^{-1} at a resolution of 2 cm^{-1}. The statistical analysis of amino acid data and FTIR spectra was carried out with the Mann−Whitney test.

Calcium Carbonate Overgrowth Experiments. Transversal sections of coral skeletons, placed in a microplate for cellular culture (MICROPLATE 24 well with Lid, IWAKI) or in a Petri dish (d = 3.2 cm), were overlaid with 750 or 3360 μL of 10 mM $CaCl_2$ solution, respectively, according to previous experiments.[10] A 30 × 30 × 50 cm^3 crystallization chamber was used. Two 25 mL beakers half-full of $(NH_4)_2CO_3$ (Carlo Erba) covered with Parafilm with 10 holes and two Petri dishes (d = 8 cm) full of anhydrous $CaCl_2$ (Fluka) were put inside the chamber. The crystallization time was 4 days. At the end of the precipitation process the transversal sections were lightly rinsed with milli-Q water (resistivity 18.2 MΩ cm at 25 °C; filtered through a 0.22 μm membrane), dried, and examined by scanning electron microscopy (SEM).

Calcium Carbonate Crystallization Experiments. The same crystallization chamber utilized for overgrowth experiments, containing $(NH_4)_2CO_3$ and anhydrous $CaCl_2$, was used. Microplates for cellular culture containing a round glass coverslip in each well were used. In each well, 750 μL of 10 mM $CaCl_2$ solutions ($CaCl_2 \cdot 2H_2O$, Merck) or of modified (increased of 10 times the Ca^{2+} and Mg^{2+} concentration) artificial seawater (ASW)[47], were poured. In the first sets of experiments, OM fractions, separately or together, were added

dx.doi.org/10.1021/cg5003572 | Cryst. Growth Des. 2014, 14, 4310−4320

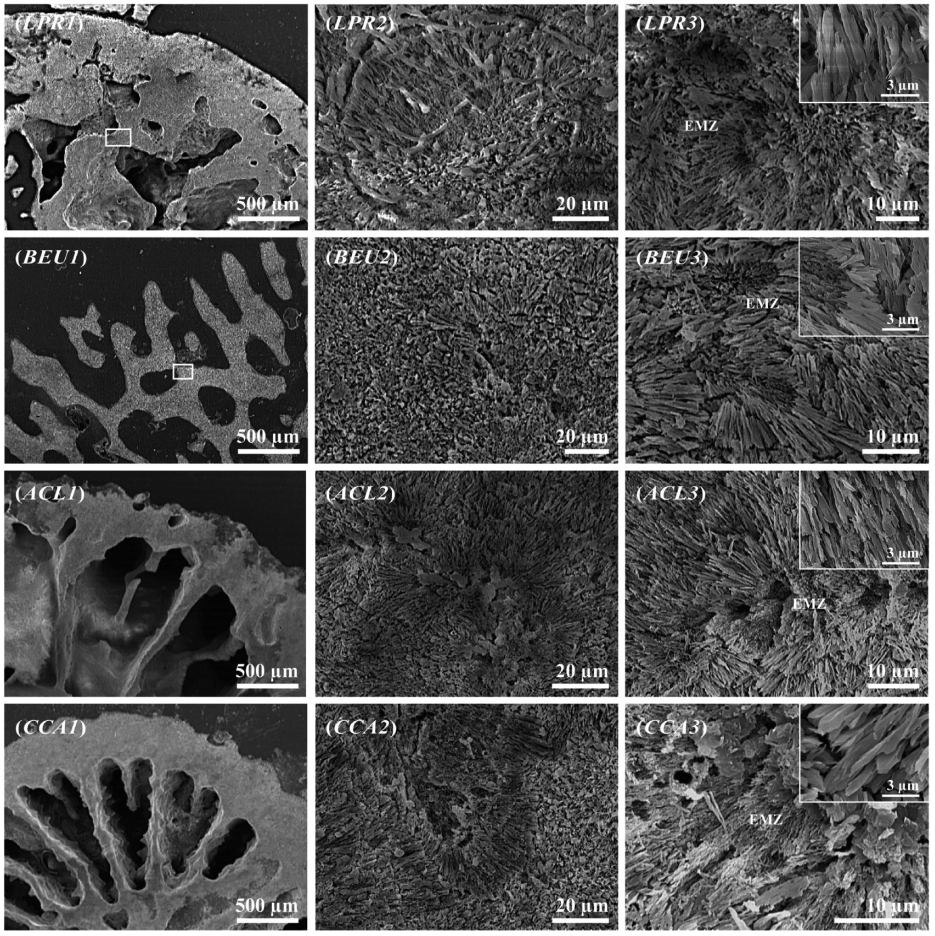

Figure 1. SEM pictures at increasing magnifications (1−3) of sections of coral skeleton of *L. pruvoti* (*LPR*), *B. europaea* (*BEU*), *A. calycularis* (*ACL*) and *C. caespitosa* (*CCA*) after etching. The pictures with suffix 3 show early mineralization zones (EMZ) surrounded by fibers, which are shown in the insets at higher magnifications.

to 750 μL of 10 mM $CaCl_2$ solution. Eight μL (for *L. pruvoti* and *A. calycularis*) or 20 μL (for *B. europaea* and *C. caespitosa*) of a solution obtained dissolving lyophilized SOM in water (17.5 mg/mL) were added to the solution. This quantity was chosen by keeping in consideration SOM concentration in the skeleton.[10,31] In other wells 0.5 mg of IOM were added to 750 μL of 10 mM $CaCl_2$ solution. SOM and the IOM (*e*OM) were added in the last wells. In the second set of experiments the whole OM (*w*OM) was added to 750 μL of 10 mM $CaCl_2$ solution and to ASW. The quantity of *w*OM added was 0.4 and 0.2 mg, respectively. The experiment proceeded for 4 days. The obtained crystals were washed three times with milli-Q water and then analyzed. All the experiments were conducted at room temperature. The crystallization trials of calcium carbonate in the different conditions were replicated starting from different batches of OM fractions.

Characterization of $CaCO_3$ Precipitates. FTIR spectra of samples in KBr disks were collected at room temperature by using a FTIR Nicolet 380 Thermo Electron Corporation working in the range of wavenumbers 4000−400 cm^{-1} at a resolution of 2 cm^{-1} according to a reported procedure.[10]

Atomic absorption measurements of calcium and magnesium were carried out with a PerkinElmer AAnalyst 100 flame and graphite furnace (HGA 800) spectrometer equipped with a Zeeman effect background corrector, and an automatic data processor. A 20-μL volume sample solution obtained by precipitated dissolution in 0.1 M HNO_3, was injected by an auto sampler. A multi-element hollow cathode lamp of analytes was used as a radiation source. Three measurements were carried out for each sample.

Thermal Treatment of $CaCO_3$ Precipitates. The samples that showed the presence of ACC in the precipitate from ASW solution with *w*OMs were heated at 105° for 18, 36, and 72 h.[48] At the end the same samples were heated at 300 °C for 8 h. FTIR spectra were collected after each thermal treatment.

Microscopic Observations. A Leica microscope equipped with a digital camera was used for optical microscope observations of $CaCO_3$ precipitates. SEM observations were conducted using a scanning electronic microscope Phenom microscope (FEI) or a Hitachi FEG 6400 scanning electron microscope after sample coating with gold.

RESULTS

Skeletal Structures of Corals. Scanning electron microscope images of septum cross sections showed the typical textural pattern of the coral skeleton (Figure 1): the EMZ was composed of small rounded granules, and fibers are produced with a patterned growth. EMZs are more sensitive to acidic etching than the fibers[49] and thus appear rich with cavities. Size and spatial distribution of EMZs and fibers vary upon species. In *L. pruvoti* and *B. europaea* the EMZs were observed as shallow cavities from which fibers radially extend having in *L. pruvoti* a smaller diameter and a less compact structure than in *B. europaea* (Figure 1 *LPR*1−3 and *BEU*1−3). In *A. calycularis* in the EMZs were observed as granular particles that cover the fiber tips. In *A. calycularis* and *C. caespitosa* the cavities are deep and episodically aligned parallel to the long axis of the septa and

dx.doi.org/10.1021/cg5003572 | *Cryst. Growth Des.* 2014, 14, 4310−4320

Table 1. Summary of the *in Vitro* Calcium Carbonate Crystallization Experiments[a] in the Presence of Organic Matrix (OM) Extracted from *L. pruvoti*, *B. europaea*, *A. calycularis*, and *C. caespitosa*

	OM composition			$CaCO_3$ overgrowth		$CaCO_3$ precipitation				
medium				10 mM $CaCl_2$		10 mM $CaCl_2$				ASW
species		SOM[e]	IOM[e]	C	A	SOM (C)	IOM (C)	*e*OM (C, A)[g]	*w*OM (C, A)[g]	*w*OM (ACC[h], MgC, A)
LPR *sol. azo.*	2.5 ± 0.1[b]	*p* (=)	*p* (=)	s. cryst.	needle bundles (1−3)[f]	db., s. ag.	cr. ag.	s. ag.	**cr. ag.**, s. ag.	nanoparticles[I]
	0.3[c]	*s* (−)	s (+)	{10.4}		(s. m. layers)	{10.4} {10.8}	(ag. nano p.)	(ag. nano p.)	2D struct.
	−[d]	*l* (=)	l (=)	(7−29)[f]		(5−57)[f]	(12−72)[f]	(5−32)[f]	(3−28)[f]	ACC1 (19.8 ± 0.5)
BEU *sol. zoo.*	2.9 ± 0.1[b]	*p* (=)	*p* (=)	**s. cryst.**	prisms (0.3−1)[f]	db., s. ag.	cr. ag.	flat. ag.[g]	**cr. ag.**, flat. ag.	nanoparticles
	1.5[c]	*s* (−)	*s* (+)	**{10.4}{hk.0}**		(add. part.)	{10.4}{10.8}	(ag. nano p.)	(ag. nano p.)	3D struct.
	+[d]	*l* (=)	*l* (=)	(6−33)[f]		(2−20)[f]	(16−53)[f]	(3−10)	(38−124)[f]	ACC2 (20.3 ± 0.6)
ACL *col. azo.*	2.7 ± 0.1[b]	*p* (=)	*p* (=)	s. cryst.	fused prisms (2−5)[f]	db., s. ag.	s. cr.	ag.	**cr. ag.**, ag.	nanoparticles
	0.2[c]	*s* (−)	*s* (+)	{10.4}		(add. part.)	{10.4} {10.8}	(ag. nano p.)	(ag. nano p.)	3D struct.
	+[d]	*l* (−)	*l* (+)	(10−50)[f]		(4−40)[f]	(4−21; 113−139)[f]	(37−68)	(7−24; 54−106)[f]	ACC2 (19.4 ± 0.5)
CCA *col. zoo.*	2.5 ± 0.1[b]	*p* (=)	*p* (=)	**s. cryst.**	fused prisms (1−4)[f]	db., s. ag.	cr. ag.	s. ag.	**cr. ag.**, s. ag.	nanoparticles
	0.3[c]	*s* (−)	*s* (+)	**{10.4} {*hk*0}**		(ag. nano p.)	{10.4}{10.8}	(ag. nano p.)	(ag. nano p.)	2D struct.
	−[d]	l (−)	l (+)	(4−28)[f]		(7−10)[f]	(26−85)[f]	(3−16)[f]	(10−42)[f]	ACC1 (19.6 ± 0.5)

[a]The main features of the OM fractions are also reported. [b]Mass percentage of OM entrapped in the skeleton. [c]Mass ratio between SOM and IOM. This data showed a great variability from one experiment to another, and the median value is reported. [d]Relative content of acidic amino acid between SOM and IOM: (+) indicates higher and (−) indicates lower. [e]*p*, *s*, and *l* indicate protein, sugars, and lipids, respectively, and their relative content between SOM and IOM is evaluated as higher (+), equal (=), or lower (−). [f]Indicates the range of dimension of the particles (in μm). [g]Only in the presence of BEU was the precipitation of aragonite observed. [h]Two forms of ACC were observed, having the FTIR ν_2 band at 868 cm^{-1} (ACC1) and 871 cm^{-1} (ACC2). In parentheses the magnesium content with respect to calcium as mol percentage is reported. [I]The presence of few elongated rhombohedral single crystals and aggregates of needle-like crystals (only BEU) was observed. When indicated, the errors are reported as standard deviations.

dx.doi.org/10.1021/cg5003572 | Cryst. Growth Des. 2014, 14, 4310−4320

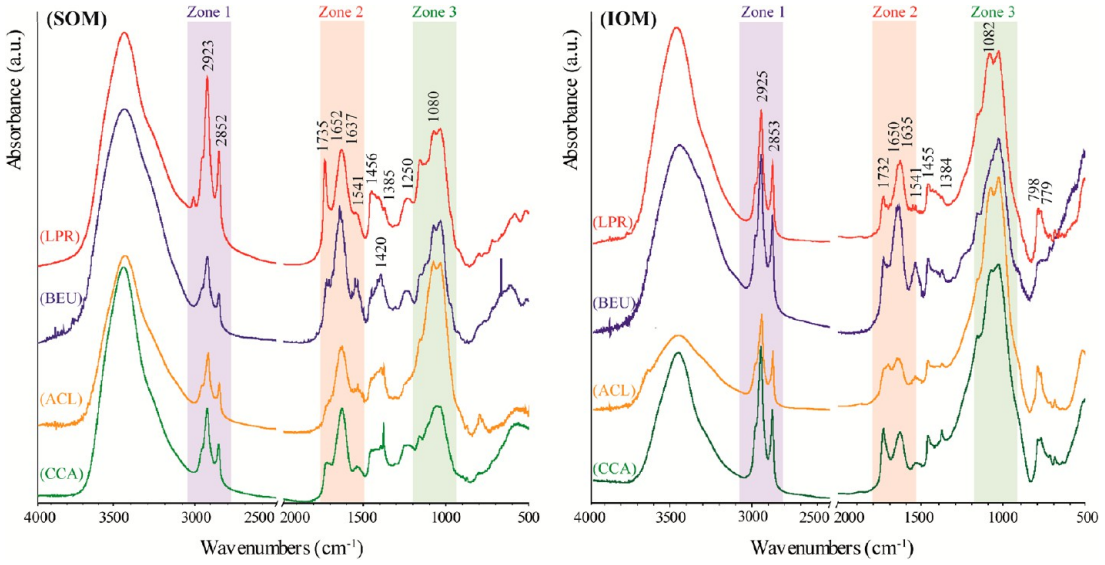

Figure 2. FTIR spectra of intraskeletal soluble (SOM) and insoluble (IOM) organic matrix from aragonitic skeleton of *L. pruvoti* (LPR), *B. europaea* (BEU), *A. calycularis* (ACL), and *C. caespitosa* (CCA). The wavenumbers of the main absorption bands are indicated. The three marked zones define diagnostic regions of functional groups, which could be mainly associated with the presence of lipids (zone 1), protein and polysaccharides (zone 2), and polysaccharides (zone 3).

the fibers are similar to those of *B. europaea* (Figure 1 *ACL*1−3 and *CCA*1−3).

Studies on the Intraskeletal OM. In *L. pruvoti*, *B. europaea*, *A. calycularis*, and *C. caespitosa* the mineral skeleton hosting the OM was expected to be of pure aragonite (Figure SI1 in the Supporting Information [SI]); however, in the insoluble residue obtained after decalcification, few silica needles were observed, constantly in *A. calycularis* and rarely in the other species (Figure SI2 in SI). The presence of this impurity, which was not possible to remove, was considered not influencing the calcium carbonate precipitation assays. The skeleton TGA showed a first weight loss (bounded water) in the range 150−220 °C followed by a second one (OM pyrolysis) between 280 and 450 °C (Figure SI3 in SI).[50] The overall weight loss was 3.4 ± 0.1, 3.9 ± 0.1, 3.5 ± 0.1, and 3.4 ± 0.1% (*w*/*w*) in *L. pruvoti*, *B. europaea*, *A. calycularis*, and *C. caespitosa*, respectively (Table1, OM composition). After extraction the OM separated in SOM and IOM fractions; the median amount of IOM was higher than that of SOM in all species, except in *B. europaea* (Table 1, OM composition).

The OM fractions were analyzed by FTIR, SDS-PAGE, and AAA. Table SI1 in SI summarizes the observations from the FTIR spectra of SOM and IOM (n = 6) and in Figure 2 the most representative spectra are shown. In SOM and IOM the same absorption bands were detected with different relative intensities (according to refs 8, 10, and 31). To estimate the relative amounts of the main molecular components of the OM from the FTIR spectra, three zones (1−3) were defined (Figure 2, Table SI3 in SI).[10] In the zone 1 (3000−2800 cm^{-1}) the bands were related to fatty acids or to molecules bearing alkylic chain regions, in the zone 2 (1750−1500 cm^{-1}) were located the bands associated to proteins (and some sugars), and in the zone 3 (1100−950 cm^{-1}) bands linked to polysaccharides.[51] The integrated intensities of the bands in zones 1 and 3 were normalized to that of zone 2 (Table SI3 in SI). Then a Mann−Whitney test was carried out to check for significant differences between SOM and IOM. In all the species SOM showed a lower absorption than IOM in the zone 3, and only in *A. calycularis* and *C. caespitosa* in the zone 1. Comparing OM fractions among all the species, the absorption of IOM from *A. calycularis* is the highest.

SDS-PAGE observations (Figure 3) of SOMs showed many bands gathered around 45 and 30 kDa in *L. pruvoti* and bands

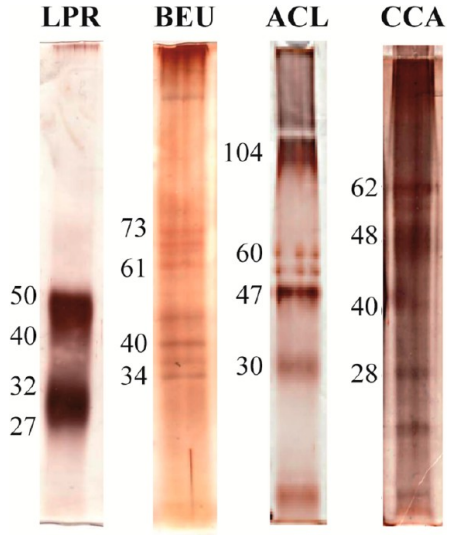

Figure 3. SDS-PAGE of intracrystalline soluble organic matrix extracted from aragonitic skeleton of *L. pruvoti* (LPR), *B. europaea* (BEU), *A. calycularis* (ACL), and *C. caespitosa* (CCA). The side numbers indicate the molecular weight (kDa) of silver stain marked bands.

clustered in two groups having molecular masses from ∼40 to 34 kDa and from 73 to 60 kDa[31] in *B. europaea*. In *A. calycularis* and *C. caespitosa* many bands distributed from ∼104 to 30 kDa and from 62 to 28 kDa, respectively, were revealed.

The AAA from SOM and IOM was reported in Table SI2 in SI. SOM was characterized by a content of aspartic (and asparagine) higher than that in IOM. The content of hydrophobic residues was always higher in IOM (33−50 mol

dx.doi.org/10.1021/cg5003572 | *Cryst. Growth Des.* 2014, 14, 4310−4320

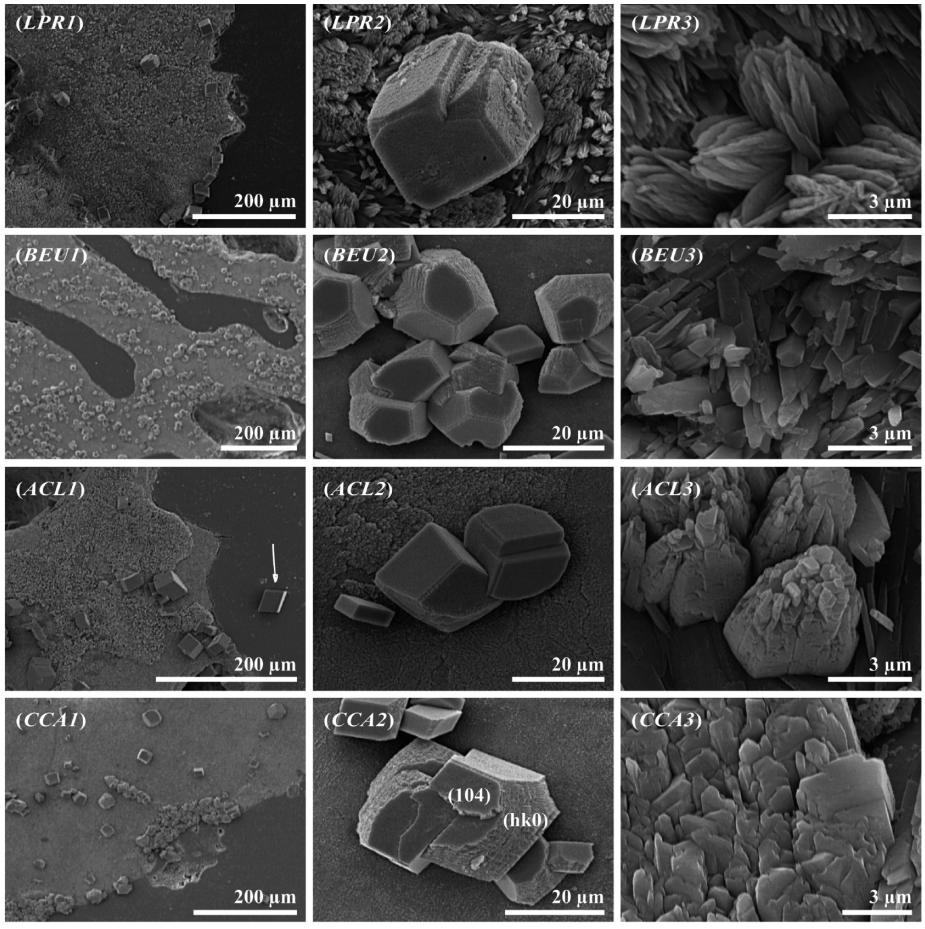

Figure 4. SEM pictures at increasing magnifications (1−3) of sections of coral skeleton of *L. pruvoti* (*LPR*), *B. europaea* (*BEU*), *A. calycularis* (*ACL*), and *C. caespitosa* (*CCA*) after calcium carbonate overgrowth experiments. A new layer of crystals with aragonite typical morphology grew on the skeleton surfaces in all the species (magn. 3). On these new layers more or less smoothed calcite crystals were observed (magn. 2) that in some cases they showed additional {*hk*0} faces to the rhombohedral {10.4}. Outside the skeletons sections only rhombohedra of calcite precipitated (*ACL1*, indicated by the arrow).

%) than in SOM (24−34 mol %). The calculated average protein pI[46] shows that OMs were acidic, and IOM was less acidic than the SOM within a species (Figure SI4 in SI).

Overgrowth of $CaCO_3$ onto Coral Skeleton Sections. The results of the calcium carbonate overgrowth experiments on skeleton cross sections are illustrated in Figure 4. Surfaces normal to the oral−aboral axis and close to the growing tips were used. The overgrowth occurred in a 10 mM calcium chloride solution under diffusion of ammonium carbonate vapors. Calcium carbonate crystals were observed on the skeleton cross section and outside it (on the surface of the embedding resin). On the resin only calcite crystals appearing almost as perfect {10.4} faced rhombohedra (see Figure 4 *ACL1* on the right) were observed. The crystals with the typical morphology of aragonite were observed only on the surface of the skeletons. They appeared as bundles of needle-like crystals in *L. pruvoti* and as single hexagonal prisms in *B. europaea*, the bundles were about 3 μm in diameter, while the needle-like crystals and the single prisms had an average diameter smaller than 1 μm. In *A. calycularis* and *C. caespitosa* the hexagonal prisms observed on *B. europaea* were coherently fused in big prisms having a diameter usually above 4 μm. On the coral skeleton calcite crystals were also observed, and they exhibited additional {*hk*0} faces to {10.4} ones, which were wider in those grown on the skeleton of *B. europaea* and *C. caespitosa* (Figure 4 *CCA2* and *BEU2*) than in those on the *A. calycularis* and *L. pruvoti* skeletons (Figure 4 *ACL2* and *LPR2*).

Precipitation in the Presence of OM Fractions. A first set of $CaCO_3$ precipitation trials was carried out from 10 mM $CaCl_2$ solutions containing the OM fractions. Without OM only the deposition of rhombohedral crystals of calcite was observed. The presence of OM fractions induced an inhibition of the precipitation and a reduction of the average particle sizes, as a monotone function of the additive concentration. On the basis of a set of preliminary studies and previous similar experiments[10,31] a SOM concentration of 185 μg/mL was used for *L. pruvoti* and *A. calycularis* and 455 μg/mL for *B. europaea* and *C. caespitosa*, while 666 μg/mL of IOM were dispersed in the calcium chloride solution.

The reported results are the trends observed from six precipitations trials (see Experimental Section and Table SI4 in SI). In the presence of SOM, aggregates having the shape of dumbbell and sphere were always observed (Figure 5 SOM). These particles (5−69 μm) showed surfaces formed by stacked multilayers (Figure 5 SOM *LPR*, inset) in the presence of *L. pruvoti* SOM, while with *B. europaea* and *A. calycularis* SOMs they showed (4−20 μm and 4−80 μm, respectively) smooth surfaces and were copresent with aggregates having various shapes (Figure 5 SOM *BEU* and *ACL*, inset). In the presence of *C. caespitosa* SOM the dumbbells and spherical shaped

dx.doi.org/10.1021/cg5003572 | *Cryst. Growth Des.* 2014, 14, 4310−4320

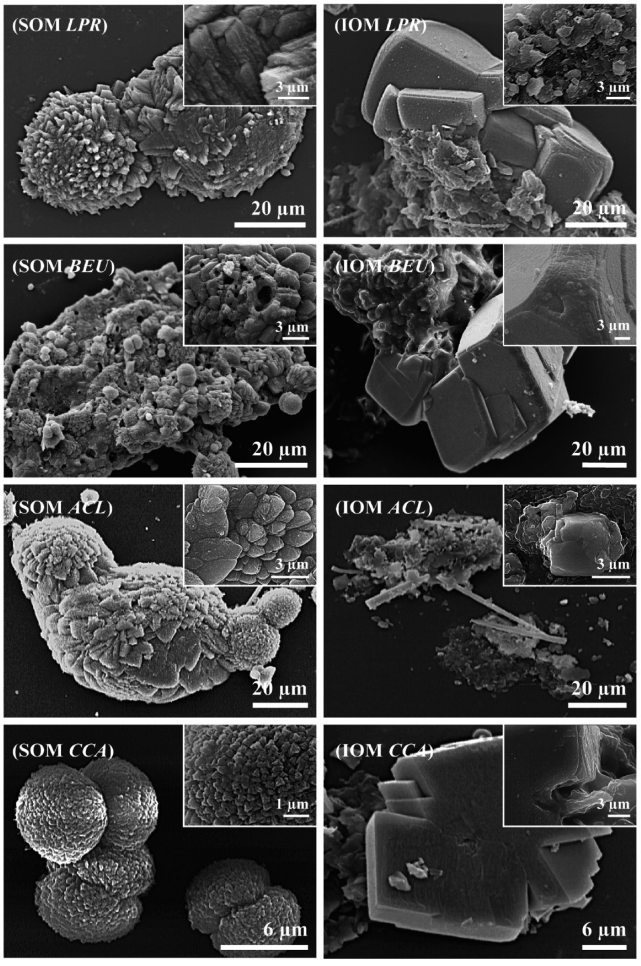

Figure 5. SEM pictures of particles obtained from precipitation experiments of $CaCO_3$ from 10 mM $CaCl_2$ solutions in the presence of OM fractions. In the first and second columns are shown particles obtained in the presence of soluble (SOM) or insoluble (IOM) organic matrix, respectively. In the rows are shown, from top to bottom, particles obtained in the presence of *L. pruvoti* (LPR), *B. europaea* (BEU), *A. calycularis* (ACL), and *C. caespitosa* (CCA). In the insets are reported high magnification pictures of the particles. The calcite crystals on IOMs show truncation of rhombohedral {104} corners and edges (probably the presence of small {108} and {*hk*0} faces). These pictures are the most representative of the populations of observed particles.

aggregates (7−80 μm) appeared formed by the association of submicrometer particles (Figure 5 SOM *CCA*, inset). The FTIR spectra of these precipitates showed the characteristic absorption bands of calcite plus those due to the SOM (Figure SI5 SOM [in SI]). In the presence of dispersed IOM, which sometime floated at the air/solution interface, the formation of mineral particles was observed both on the matrix surface and outside it. On the IOMs framework, from all the species, calcite crystals grew, showing truncation of rhombohedral corners and edges (Figure 5 IOM and insets). On *A. calycularis* IOM only a few calcium carbonate particles were observed, together with the needle-like silica contaminants (see Materials and Methods section). On *L. pruvoti*, *C. caespitosa*, and *B. europaea* IOM, and outside it, the calcite crystals assembled showing overlapping edges (Figure 5 IOM *LPR*, IOM *BEU*). The FTIR spectra showed only the presence of the absorption bands of calcite, with those of IOM (Figure SI5 IOM [in SI]).

When the *e*OM was used (Figure 6 *e*OM and inset) few aggregates formed by small particles (submicrometer size)

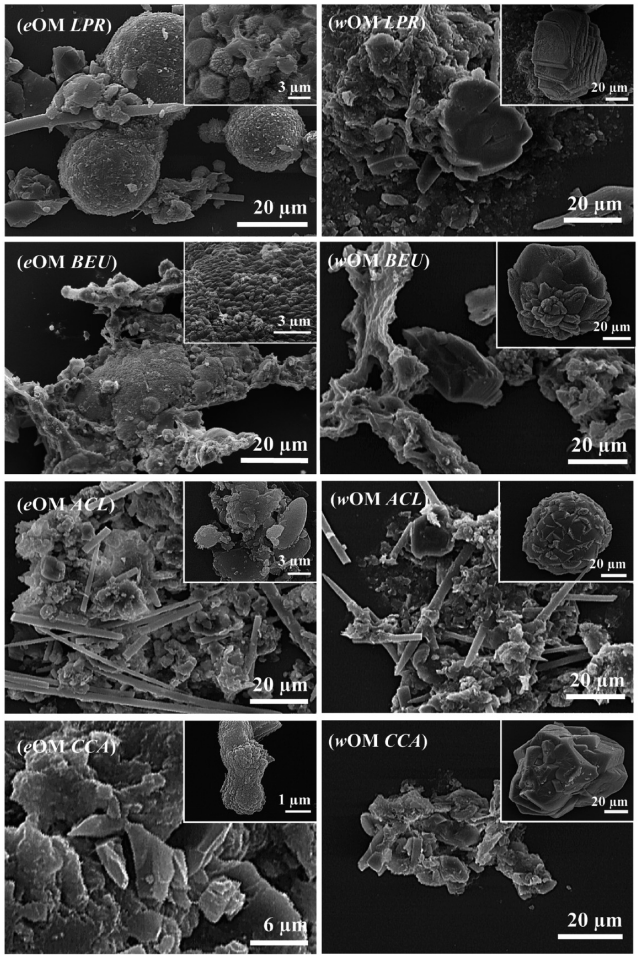

Figure 6. SEM pictures of particles obtained from precipitation experiments of $CaCO_3$ from 10 mM $CaCl_2$ solutions in the presence of the entire organic matrix (*e*OM) or the whole organic matrix (*w*OM). The *e*OM and *w*OM were extracted from *L. pruvoti* (LPR), *B. europaea* (BEU), *A. calycularis* (ACL), and *C. caespitosa* (CCA). In the picture ACL needle-like silica spicules are present. In the insets are reported high magnification images of representative features of the associated particles. These pictures are the most representative of the populations of observed particles.

precipitated; this observation effect was prominent for *A. calycularis*. In the presence of *L. pruvoti*, *B. europaea*, and *C. caespitosa* *e*OM, the surface of the IOM was covered by aggregates of submicrometer units having a rough surface. In addition, crystals, like those precipitated in the presence of SOM, were observed around the IOM, particularly for *C. caespitosa* (Figure 6 *e*OM *CCA* inset). In the presence of *A. calycularis* *e*OM few aggregates with shape changing from one experiment to another were observed (the most representative in Figure 6 *e*OM *ACL*). The FTIR spectra of these materials (Figure SI5 *e*OM [in SI]) showed the absorption bands of calcite, except for *B. europaea* where the aragonite bands were observed as well (as reported in ref 31).

Precipitation in the Presence of the Whole OM. A second set of $CaCO_3$ precipitation trials, in which the *w*OM was added into a 10 mM $CaCl_2$ solution or into an ASW[47] solution (Figure 6, Table 1 and Table SI4 in SI), was carried

dx.doi.org/10.1021/cg5003572 | *Cryst. Growth Des.* 2014, 14, 4310−4320

out. The experiments were carried out using 0.25 or 0.5 mg/mL of *w*OM, but the latter inhibited the precipitation over 4 days.

From the 10 mM $CaCl_2$ solution containing *w*OM precipitated $CaCO_3$ particles (Figure 6 *w*OM) similar to those observed in the presence of *e*OM (Figure 6 *e*OM) but showing morphological features closer to those observed in the presence of the respective IOM (Figure 5 IOM).

From the precipitation in ASW, aggregates having the shapes of peanut, dumbbell, and spherulite and formed by submicrometer-sized elongated rhombohedral crystals and needle-like crystals were observed (Figure 7 ASW). These aggregates were formed of magnesium calcite and aragonite (Figure 8a). The addition of the *w*OM to the ASW produced the massive precipitation of spherical submicrometer particles (Figure 7 ASW + *w*OM) and of few elongated rhombohedral crystals and needle-like crystals (only BEU). The aggregation of the submicrometer particles was species specific. They appeared as forming long chains associated in a two-dimensional network for *L. pruvoti* and *C. caespitosa*, while for *B. europaea* and *A. calycularis* three-dimensional architectures were generated. The FTIR spectra showed the presence of the typical absorption bands of ACC.[52] The presence of ACC was also verified by X-ray powder diffraction (Figure SI7 in SI). The diffraction pattern of the precipitates obtained in the presence of *w*OM showed only diffraction peaks due to the presence of halite and a very weak broad peak at about 29.7°. From ASW, diffraction peaks owing to aragonite and magnesium calcite were observed. Despite these observations the presence of traces of hydrated forms of calcium carbonate could not be excluded. ACC was further investigated by FTIR experiments upon thermal treatment of the precipitates (Figure 8 and Table SI5 in SI). The ν_3 and ν_2 showed a different position and profile bands after the thermal treatments. In the ACC obtained from *L. pruvoti* and *C. caespitosa* the ν_2 band was at 868 cm^{-1}, and in the ones from *B. europaea* and *A. calycularis* the band was at 871 cm^{-1}. Upon thermal treatment at 105 °C for 18 h for all the ACC the ν_2 band was at 871 cm^{-1}, and after 76 h this band moved to 875 cm^{-1} for all the samples, the same value showing in the precipitate formed from ASW without OM. When the same samples were thermally treated for 8 h at 300 °C they all showed the ν_2 band at 877 cm^{-1}. Moreover, a second band at 860 cm^{-1} clearly appeared in the precipitate obtained from *B. europaea*, analogous to that obtained from pure ASW, and was present as a shoulder in *A. calycularis* precipitate. The profile of the ν_3 band showed three main maxima centered at 1431, 1466, and 1480 cm^{-1}. By thermal treatment the maximum at 1431 cm^{-1} strengthened, while the one at 1480 cm^{-1} weakened. This change in intensities was more difficult in *B. europaea* that in the other species. The analysis of the absorption band at about 3300 cm^{-1}, due to the OH groups stretching, did not reveal any clear trend. This difficulty can be ascribed to the diverse contributions (e.g., water solvatation, carbohydrates) to this band and the presence of moisture. In the precipitates from the ASW the Mg/Ca molar ratio was measured by the atomic absorption spectroscopy ($n = 6$). These were 19.8 ± 0.5, 20.3 ± 0.6, 19.4 ± 0.5, and 19.6 ± 0.5 in *L. pruvoti*, *B. europaea*, *C. caespitosa*, and *A. calycularis*, respectively, while in the absence of OM it was 5.1 ± 0.1 (Table 1).

DISCUSSION

The precipitation of aragonite in corals occurs in a confined environment in a seawater-like fluid that contains biomineralizing (macro)molecules.[25,53] The understanding of the role of seawater ions (mainly magnesium) and of biomineralizing macromolecules in the *in vivo* calcification process lays objective difficulties, although terrific results were achieved.[54] The *in vitro* mineral precipitation in the presence of OM components represents an alternative approach. This assay has the disadvantage, and limitation, that only intraskeletal macromolecules upon an extraction process are considered. However, the assay was validated by a plethora of studies that have proved that the intraskeletal macromolecules were effective modifiers

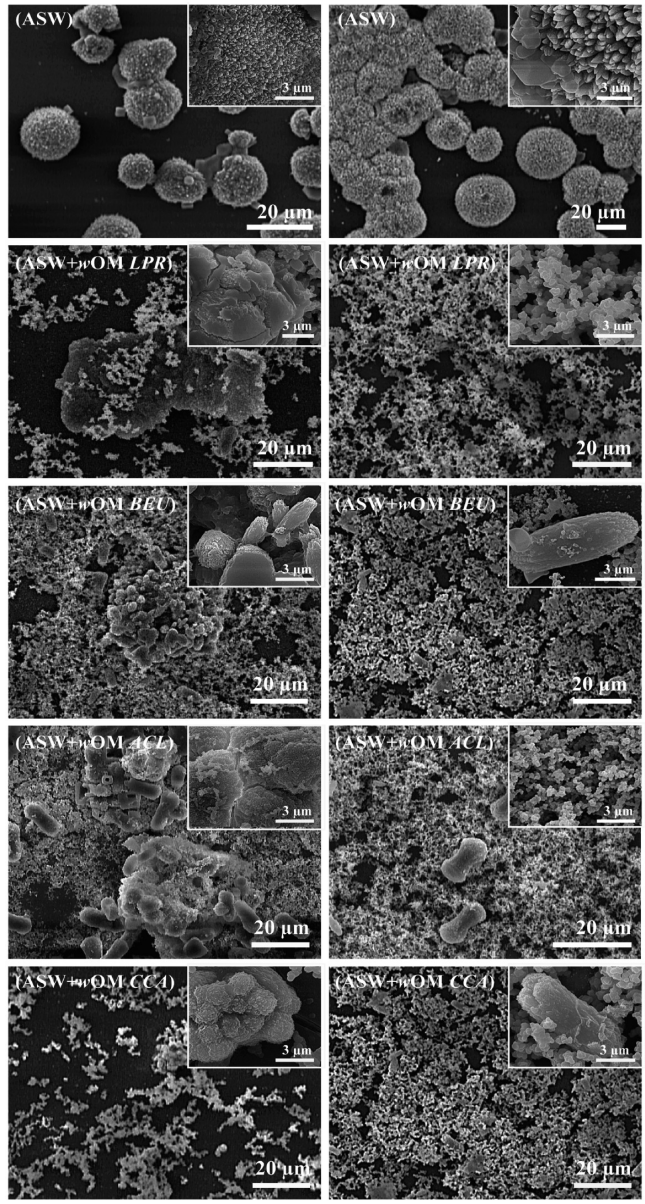

Figure 7. SEM pictures of particles obtained from precipitation experiments of $CaCO_3$ from artificial seawater (ASW) in the presence of the whole organic matrix (*w*OM), after the synthesis (left), and after the thermal treatment at 300 °C for 12 h (right). The spherical nanoparticles (2nd–4th row) were made of ACC before the thermal treatment and of magnesium calcite after the thermal treatment. In the presence of the *w*OM from *B. europaea*, aragonite coformed with magnesium calcite. The *w*OM was extracted from *L. pruvoti* (LPR), *B. europaea* (BEU), *A. calycularis* (ACL), and *C. caespitosa* (CCA). These pictures are the most representative of the populations of observed particles.

dx.doi.org/10.1021/cg5003572 | *Cryst. Growth Des.* 2014, 14, 4310–4320

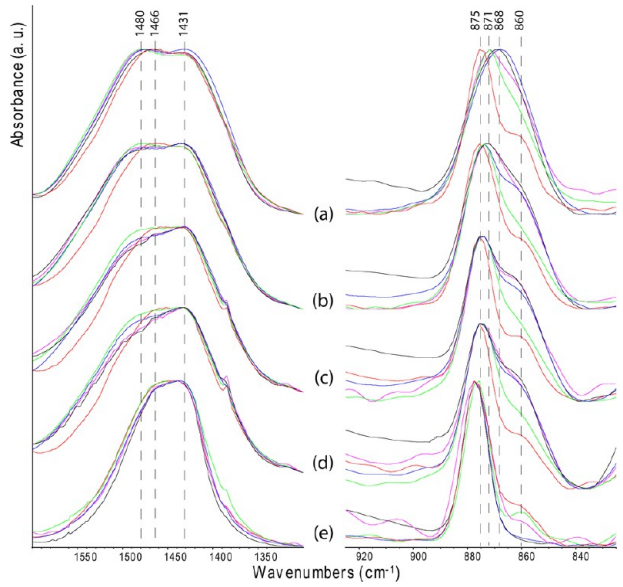

Figure 8. FTIR spectra of calcium carbonate precipitated from artificial seawater in the presence of the whole organic matrix (*w*OM), which was extracted from *L. pruvoti* (blue), *B. europaea* (green), *A. calycularis* (magenta), and *C. caespitosa* (black). The spectra from calcium carbonate precipitated from artificial seawater in the absence of *w*OM are also reported (red). Only the diagnostic ranges from 800 to 900 cm^{-1} and 1300 to 1600 cm^{-1} are shown (see SI for the entire FTIR spectra). (a) Spectra collected without any thermal treatment of the samples. (b–d) Spectra collected after a thermal treatment of the samples at 105 °C for 18 h (b), 36 h (c), and 72 h (d). (e) Spectra collected after a thermal treatment of the samples at 300 °C for 12 h.

of the nucleation and growth processes of minerals deposited by organisms.[54−56] Until few years ago this assay was almost ignored in the study of the biomineralization of corals. Recently, few *in vitro* studies have shown that the intraskeletal OM of corals influenced the aragonite precipitation.[10,31,32] Scleractinian corals, differently from many other marine calcifiers, show diverse growth forms (solitary vs colonial) and trophic strategies (zooxanthellate vs nonzooxanthellate). The presence of zooxanthellae was reported to have an influence on the calcification process.[9,42] A study on the OM amino acid composition showed differences between different species with different trophic strategies in the content of acidic residues.[35] Here, the study of the composition of OMs from the corals *L. pruvoti*, *B. europaea*, *A. calycularis*, and *C. caespitosa* showed the absence of any clear correlation among coral ecology (growth form or trophic strategy) and OM content, mass ratio between SOM and IOM, protein features, and macromolecule distribution (Table 1). An emerging feature was the high mass ratio SOM/IOM (1.5) in *B. europaea* (Table 1), a non-unique behavior since in *Acropora digitifera* a ratio of about 5 was observed.[10] Overgrowth experiments showed that aragonite formed on the surface of all coral skeletons. This effect, which could be due to secondary nucleation events, brought to the growth of crystals having species specific size and texture. On the skeleton of the zooxanthellate species, *B. europaea* and *C. caespitosa*, the overgrowth of numerous calcite crystals having a modified morphology was also observed. This can be related with the release in solution of molecules able to interact specifically with the {*hk*0} faces of calcite.[28] The band's distribution revealed by SDS-PAGE seemed to exclude that this effect was related to the presence of a significant amount of low-molecular weight molecules more easily released from the skeleton, keeping in consideration that some molecules could be not stained or fixed by the gel.[57] The calcium carbonate precipitation experiments in the presence of SOM, IOM, and the *e*OM gave results in agreement to what is observed for other coral species.[10,31] The SOM molecules were strong modifiers of the morphology of the calcite particles. These changes in morphology were due either to the aggregation of modified single-crystalline units of calcite, as in case of *L. pruvoti*, *A. calycularis*, and *C. caespitosa*, or to the assembly of submicrometer particles, as for *B. europaea*. The presence of IOM lightly affected the precipitation of calcite, and the crystals were slightly modified from their rhombohedral morphology, suggesting the limited release of IOM molecules in solution, favored by the crystallization conditions (pH and ionic strength).[10,31] According to reported data[10,31] the *e*OM effect on the precipitation was dominated by the SOM fraction, except for *B. europaea* where the copresence of SOM and IOM allowed the precipitation of aragonite together with calcite in a Mg-ion-free $CaCl_2$ solution, where usually calcite precipitated.[31] The favored precipitation of aragonite by OM molecules has been observed also for *Stylophora pistillata*,[32] but these experiments were carried out in seawater where the presence of magnesium ions (Mg/Ca molar ratio equal to 5) favors the precipitation of aragonite. The trials in which the *w*OM was used instead of *e*OM were performed to exclude possible artifacts associated with the separation process between SOM and IOM (e.g., reaggregation and reprecipitation). The results with *w*OM were in line with those obtained using *e*OM, but the morphological effects were more similar to those observed in the presence of IOM, suggesting that in the *w*OM a lower content of SOM was present with respect to the *e*OM.

More information with respect to what is already known was obtained from precipitation experiments in ASW using the *w*OM. In fact, previously described experiments showed that *w*OM behaved similarly to *e*OM, and it was definitely more representative of the OM entrapped in the skeleton. These two OMs differed for the extraction mode. In the *e*OM experiments the soluble and insoluble organic matrices were separated during the extraction process and then used together; with the *w*OM extracted in one step. The fact that these two procedures gave materials having similar functions in the precipitation of calcium carbonate indicated that (i) the activity of soluble and insoluble fractions was not affected by the extraction process and that (ii) the interaction between soluble and insoluble fractions was a reversible process. The use of ASW was in line with recent researches showing direct seawater transport to the calcifying site in corals.[25] The presence of magnesium ions in the extracytoplasmic calcifying fluid, at the nucleation site of corals, has been also reported.[47,58,59] The addition of *w*OM to ASW induced the precipitation of almost only ACC instead of aragonite and Mg-calcite, as revealed by the FTIR and X-ray diffraction analyses. ACC appeared in two forms having different FTIR spectra and thermal stabilities. The thermally less stable form of ACC, which precipitated in the presence of *w*OM from *L. pruvoti* and *C. caespitosa*, converted in the one more stable, which precipitated in the presence of *w*OM from *B. europaea* and *A. calycularis*, upon heating at 105 °C for 18 h. According to Radha et al.[60] a hydrated ACC transformed with aging or heating into a less hydrated form, crystallizing with time as calcite or aragonite. Two ACC forms, anhydrous ACC and hydrated ACC containing about 1 mol of water that persists for longer time periods, exist in biogenic sources.[61]

dx.doi.org/10.1021/cg5003572 | *Cryst. Growth Des.* 2014, 14, 4310−4320

Thus, we could infer that in our experiment the ACC thermally less stable forms (probably the hydrated ACC) converted to less hydrated, or anhydrous, ones upon heating (the complexity of the material did not allow accurate thermal analyses). The less hydrated ACC showed a different behavior when subject to a further heating process. It converted to poor crystalline Mg calcite in the presence of *w*OM from *L. pruvoti*, *A. calycularis*, and *C. caespitosa*, while the one from *B. europaea* formed Mg calcite and aragonite (Table SI5 in SI). This polymorphic selectivity in the solid-state crystallization of the ACC was attributed to the *w*OM, since the same heating profile was used, excluding effects due to the annealing rate.[62] Moreover, an increase in the crystallinity of Mg-calcite was observed after annealing.[48] The existence of two forms of ACC, which had a diverse binding strength, was reported as precursors of diverse crystalline phases.[63]

The wet transition from ACC to specific crystalline phases was reported to rely on the Mg/Ca molar ratio and the presence of additives in the precipitating solution.[64−67] In particular it was observed that in conditions of the Mg/Ca molar ratio >4 the transition from ACC to aragonite[64] occurred through monohydrocalcite at transition phase[67] in times shorter (<4 days) than those used in this study. This strongly indicated a stabilization of the ACC by the *w*OM; indeed in its absence, the ACC precipitation was not observed.

It has been reported that the formation and stability of different hydrated ACC forms have been ascribed to the copresence of Mg ions and OM from diverse mineralized tissues.[52,68] However, our data suggest that *w*OM plays a primary role in the ACC formation. Here, the *w*OM stabilization of two forms of ACC was not related to the content of Mg^{2+} hosted in ACC, being the same in all the precipitates (Table 1). Moreover, the coprecipitation of ACC with crystalline phases was observed also in the absence of magnesium ions.

The stabilization of ACC by *w*OM suggested that also coral biomineralization followed a crystallization pathway involving the formation of a transient form, as reported for foraminifera, mollusks, and echinoderms.[30] This agreed with recent observations on growing corals that reported the presence of transient granules that convert to aragonite fibers.[16] However, the presence of ACC was not detected in coral recruits.[69]

CONCLUSIONS

In conclusion, this research added three important observations to the study on *in vitro* precipitation of calcium carbonate: (i) the capability of OM to affect morphology and polymorphism was not related to the coral growth form or trophic strategy; (ii) in simulated seawater the OM stabilized the formation of diverse forms of ACC which converted species specifically in aragonite or magnesium calcite upon thermal treatment; (iii) *B. europaea* showed distinguished *in vitro* biomineralization features. Under overgrowth and solution precipitation experiments, its OM was the most prone to favor the precipitation of aragonite in the absence of magnesium ions; under thermal treatments, its ACC was unique, with being the most stable, and was the only one that partially converted to aragonite instead of magnesium calcite. These features suggested a stronger control of *B. europaea* OM over the mineral phases and a higher independence from crystallization environment compared to the other species. The reasons for the peculiar behavior of the OM from *B. europaea* were unknown. However, this species is distinguished also for its ecological properties, being the only one able to tolerate the effects of ocean acidification.[70]

ASSOCIATED CONTENT

Supporting Information

Experimental details on the X-ray powder pattern, FTIR spectra, TGA analyses, amino acid analyses, aliphatic index, and isoelectric point. This material is available free of charge via the Internet at http://pubs.acs.org.

AUTHOR INFORMATION

Corresponding Authors

*E-mail: s.goffredo@unibo.it. Telephone: +39 051 20994244.
*E-mail: giuseppe.falini@unibo.it. Telephone: +39 051 2099484.

Author Contributions

G.F., S.G., J.-P.C, Y.D, and Z.D. conceived and designed the project. M.R, V.L., F.S., and Y.D. carried out the experiments. All the authors contributed to data analysis, scientific discussion, and the writing of the paper. All authors have given approval to the final version of the manuscript.

Notes

The authors declare no competing financial interest.

ACKNOWLEDGMENTS

The research leading to these results has received funding from the European Research Council under the European Union's Seventh Framework Programme (FP7/2007-2013)/ERC Grant Agreement No. [249930-CoralWarm: Corals and global warming: the Mediterranean versus the Red Sea; www.CoralWarm.eu]. G.F. and S.F. thank CIRC-MSB for support. S.G. thanks S. Branchini, S. Guerrieri, and M. Marinozzi for help in collecting the samples. We thank Gianni Neto for the underwater picture of *A. calycularis*.

REFERENCES

(1) Spalding, M. D.; Ravilious, C.; Green, E. P. *World Atlas of Coral Reefs*; University of California Press: Berkeley, 2001; pp 424.
(2) Cohen, A. L.; McConnaughey, T. A.; Dove, P. M.; Weiner, S.; Yoreo, J. J. Geochemical perspectives on coral mineralization. *Biominer., Rev. Miner. Geochim.* **2003**, 151−187.
(3) Marshall, A. T.; Clode, P. *Coral Reefs* **2004**, *23*, 218−224.
(4) Allemand, D.; Tambutté, È.; Zoccola, D.; Tambutté, S. Coral calcification, cells to reefs. In *Coral reefs: and ecosystem in transition*; Dubinsky, Z., Stambler, N, Eds.; Springer: Dordrecht, 2011; pp 119−150.
(5) Jokiel, P. F. *J. Exp. Mar. Biol. Ecol.* **1978**, *35*, 87−97.
(6) Jokiel, P. F.; Coles, S. L. *Coral Reefs* **1990**, *8*, 155−162.
(7) Kuffner, I. B.; Andersson, A. J.; Jokiel, P. L.; Rodgers, K. S.; Mackenzie, F. T. *Nature Geosci.* **2008**, *1*, 114−117.
(8) Cuif, J.-P.; Lecointre, G.; Perrin, C.; Tillier, A.; Tillier, S. *Zool. Scr.* **2003b**, *32*, 459−473.
(9) Tambutté, S.; Holcomb, M.; Ferrier-Pagès, C.; Reynaud, S.; Tambutté, É.; Zoccola, D.; Allemand, D. *J. Exp. Mar. Biol. Ecol.* **2011**, *408*, 58−78 (and references therein)..
(10) Falini, G.; Reggi, M.; Fermani, S.; Sparla, F.; Goffredo, S.; Dubinsky, Z.; Levi, O.; Dauphin, Y.; Cuif, J.-P. *J. Struct. Biol.* **2013**, *183*, 226−238.
(11) Wilfert, M.; Peters, W. *Z. Morph. Tiere* **1969**, *64*, 77−84.
(12) Young, S. D. *Comp. Biochem. Physiol.* **1971**, *40B*, 113−120.
(13) Cuif, J.-P.; Dauphin, Y. *Paläont. Z.* **1998**, *72*, 257−270.
(14) Cuif, J.-P.; Dauphin, Y.; Doucet, J.; Salome, M.; Susini, J. *Geochim. Cosmochim. Acta* **2003a**, *67*, 75−83.
(15) Vandermeulen, J. H.; Watabe, N. *Mar. Biol.* **1973**, *23*, 47−57.

(16) van de Locht, R.; Verch, A.; Saunders, M.; Dissard, D.; Rixen, T.; Moya, A.; Kroger, R. *J. Struct. Biol.* **2013**, *183*, 57−65.
(17) Addadi, L.; Moradian, J.; Shay, E.; Maroudas, N. G.; Weiner, S. *Proc. Natl. Acad. Sci. U.S.A.* **1987**, *84*, 2732−2736.
(18) Falini, G.; Albeck, S.; Weiner, S.; Addadi, L. *Science* **1996**, *271*, 67−69.
(19) Falini, G.; Fermani, S.; Tosi, G.; Dinelli, E. *Cryst. Growth. Des.* **2009**, *9*, 2065−2072.
(20) Puverel, S.; Tambutté, É.; Periera-Mouriès, L.; Zoccola, D.; Allemand, D.; Tambutté, S. *Comp. Biochem. Physiol.* **2005**, *150B*, 10−22.
(21) Constantz, B.; Weiner, S. *J. Exp. Zool* **1988**, *248*, 253−258.
(22) Dauphin, Y. *Int. J. Biol. Macromol.* **2001**, *28*, 293−304.
(23) Farre, B.; Cuif, J.-P.; Dauphin, Y. *Zoology* **2010**, *113*, 250−257.
(24) McConnaughey, T. A.; Whelan, J. F. *Earth Sci. Rev.* **1997**, *42*, 95−117.
(25) Gagnon, A. C.; Adkins, J. F.; Erez, J. *Earth Planet. Sci. Lett.* **2012**, *329*−*330*, 150−161.
(26) Clode, P. L.; Marshall, A. T. *Tissue Cell* **2002**, *34*, 187−198.
(27) Addadi, L.; Joester, D.; Nudelman, F.; Weiner, S. *Chem.—Eur. J.* **2006**, *12*, 981−987.
(28) Addadi, L.; Weiner, S. *Angew. Chem., Int. Ed. Engl.* **1992**, *31*, 153−169.
(29) Didymus, J. M.; Oliver, P.; Mann, S. *Chem. Soc., Faraday Trans.* **1993**, *89*, 2891−2900.
(30) Weiner, S.; Addadi, L. *Annu. Rev. Mater. Res.* **2011**, *41*, 21−40.
(31) Goffredo, S.; Vergni, P.; Reggi, M.; Caroselli, E.; Sparla, F.; Levy, O.; Dubinsky, Z.; Falini, G. *PLoS One* **2011**, *6*, e22338.
(32) Mass, T.; Drake, J. L.; Haramaty, L.; Kim, J. D.; Zelzion, E.; Bhattacharya, D.; Falkowski, P. G. *Curr. Biol.* **2013**, *23*, 1126−1131.
(33) Muscatine, L.; Cerchiarini, F. *Biol. Bull.* **1969**, *137*, 506−523.
(34) Johnson, I. S. *Int. Rev. Cytol.* **1980**, *67*, 171−214.
(35) Cuif, J.-P.; Dauphin, Y.; Freiwald, A.; Gautret, P.; Zibrowius, H. *Comp. Biochem. Physiol. A* **1999**, *123*, 269−278.
(36) Muscatine, L.; Goiran, C.; Land, L.; Jaubert, J.; Cuif, J.-P.; Allemand, D. *Proc. Natl. Acad. Sci. U.S.A.* **2005**, *102*, 1525−1530.
(37) Kawaguti, S.; Sakumoto, D. *Bull. Natl. Inst. Ocean Taiwan* **1948**, *4*, 65−70.
(38) Gattuso, J. P.; Allemand, D.; Frankignoulle, M. *Am. Zool.* **1999**, *39*, 160−183.
(39) Goreau, T. F. *Biol. Bull.* **1959**, *106*, 59−75.
(40) Gautret, P.; Cuif, J.-P.; Freiwald, O. *Facies* **1997**, *36*, 189−194.
(41) Pearse, V. B.; Muscatine, L. *Biol. Bull.* **1971**, *141*, 350−363.
(42) Tambutté, É.; Allemand, D.; Zoccola, D.; Meibom, A.; Lotto, S.; Caminiti, N.; Tambutté, S. *Coral Reefs* **2007**, *26*, 517−529.
(43) Marshall, A. T.; Clode, P. *J. Exp. Biol.* **2002**, *205*, 2107−2113.
(44) Al-Horani, F. A.; Al-Moghrabi, S. M.; De Beer, D. *Mar. Biol.* **2003**, *142*, 419−426.
(45) Al-Horani, F. A. *Sci. Mar.* **2005**, *69*, 347−354.
(46) Sillero, A.; Ribeiro, J. *Anal. Biochem.* **1989**, *179*, 319−325.
(47) Kester, D. R.; Duedall, I. W.; Connors, D. N.; Pytkowicz, R. M. Preparation of artificial seawater. *Limnol. Oceanogr.* **1967**, *12*, 176−179.
(48) Xu, X.; Han, J. T.; Kim, do H.; Cho, K. *J. Phys. Chem. B* **2006**, *110*, 2764−2770.
(49) Cuif, J.-P.; Dauphin, Y. *J. Struct. Biol.* **2005**, *150*, 319−331.
(50) Cuif, J.-P.; Dauphin, Y.; Berthet, P.; Jegoudez, J. *Geochem. Geophys. Geosyst.* **2004**, *5*, Q11011.
(51) Parker, F. S. *Applications of Infrared, Raman, and Resonance Raman Spectroscopy in Biochemistry*; Plenum Press: New York, 1983.
(52) Addadi, L.; Raz, S.; Weiner, S. *Adv. Mater.* **2003**, *15*, 959−970.
(53) Venn, A. A.; Tambutté, É.; Holcomb, M.; Laurent, J.; Allemand, D.; Tambutté, S. *Proc. Natl. Acad. Sci. U.S.A.* **2013**, *110*, 1634−1639.
(54) Mann, S. *Biomineralization. Principles and Concepts in Bioinorganic Materials Chemistry*; Oxford University Press: New York, 2001; Vol. *198*.
(55) Weiner, S.; Dove, P. An Overview of Biomineralization Processes and the Problem of the Vital Effect. Dove, P. M., Weiner, S., Yoreo, J. J., Eds.; In *Biominer., Rev. Miner. Geochim.* **2003**, 1−29.
(56) Meldrum, F. C.; Coelfen, H. *Chem. Rev.* **2008**, *108*, 4332−4342.
(57) Gotliv, B.-A.; Addadi, L.; Weiner, S. *Eur. J. Chem. Biol.* **2003**, *4*, 522−529.
(58) Holcomb, M.; Cohen, A. L.; Gabitov, R. I.; Hutter, J. L. *Geochim. Cosmochim. Acta* **2009**, *73*, 4166−4179.
(59) Tambutté, É.; Tambutté, S.; Segonds, N.; Zoccola, D.; Venn, A. A.; Erez, J.; Allemand, D. *Proc. Biol. Sci.* **2012**, *7*, 19−27.
(60) Radha, A. V.; Forbes, T. Z.; Killian, C. E.; Gilbert, P. U. P. A.; Navrotsky, A. *Proc. Natl. Acad. Sci. U.S.A.* **2010**, *107*, 816438−16443.
(61) Raz, S.; Hamilton, P. C.; Wilt, F. H.; Weiner, S.; Addadi, L. *Adv. Funct. Mater.* **2003**, *13*, 480−486.
(62) Noel, E. H.; Kim, Y.-Y.; Charnock, J. M.; Meldrum, F. C. *CrystEngComm* **2013**, *15*, 697−705.
(63) Gebauer, D.; Gunawidjaj, P. N.; Ko, J. Y. P.; Bacsi, Z.; Aziz, B.; Liu, L.; Hu, Y.; Bergström, L.; Tai, C.-W.; Sham, T.-K.; Edén, M.; Hedin, N. *Angew. Chem.* **2010**, *122*, 9073−9075.
(64) Zhang, Z.; Xie, Y.; Xun, X.; Pan, H.; Tang, R. *J. Cryst. Growth* **2012**, *343*, 62−67.
(65) Raiteri, P.; Gale, J. D. *J. Am. Chem. Soc.* **2010**, *132*, 17623−17634.
(66) Lam, R. S. K.; Charnock, J. M.; Lennie, A.; Meldrum, F. C. *CrystEngComm* **2007**, *9*, 1226−1236.
(67) Loste, E.; Wilson, R. M.; Seshadric, R.; Meldrum, F. C. *J. Cryst. Growth* **2003**, *254*, 206−218.
(68) Politi, Y. *Chem. Mater.* **2010**, *22*, 161−166.
(69) Clode, P. L.; Lema, K.; Saunders, M.; Weiner, S. *Coral Reefs* **2011**, *30*, 1−8.
(70) Goffredo, S.; Prada, F.; Caroselli, E.; Pasquini, L.; Fantazzini, P.; Fermani, S.; Reggi, M.; Levy, O.; Fabricius, K. E.; Dubinsky, Z.; Falini, G. *Nat. Clim. Change* **2014**, *4*, 593−597.